Hindawi
Advances in Civil Engineering
Volume 2021, Article ID 5542830, 17 pages
https://doi.org/10.1155/2021/5542830

Research Article

Instability Analysis and Reinforcement Support Technology of Coal-Rock Interbed Roadway in Gaojiazhuang Coal Mine

Chaolin Liu[1,2] **and Guohua Zhang**[1]

[1]*Heilongjiang University of Science and Technology, Haerbin, Heilongjiang 150022, China*
[2]*Information Institute of the Ministry of Emergency Management of the PRC, Chaoyang, Beijing 100029, China*

Correspondence should be addressed to Guohua Zhang; 690349626@qq.com

Received 27 January 2021; Revised 6 March 2021; Accepted 16 March 2021; Published 30 March 2021

Academic Editor: Zhijie Zhu

In order to effectively solve a series of problems such as the difficulty of coal and rock interbed roadway support in Gaojiazhuang Coal Mine and get a scientific and reasonable optimization scheme of surrounding rock support, theoretical analysis, numerical simulation, ultrasonic detection, field-effect test, and other means are adopted to analyze the instability of coal and rock interbed roadway. The results show that the interbedded roadway has weak interbedded cementation, and its ore pressure is more intense due to the influence of its interbedded weak structural plane. Based on Mohr's strength envelope principle, it is proposed that horizontal stress is the main factor that causes a wide range of shear displacement, penetration crack, and surrounding rock failure of the roof of this kind of roadway. Through the finite element numerical simulation analysis, the deformation and failure law, stress distribution characteristics, and failure area distribution characteristics of coal and rock interbedding roadway surrounding rock are theoretically revealed, and the control effect of different support schemes on roadway surrounding rock deformation is greatly different. Based on the ultrasonic detection technology, it is proved that the roadway side failure has strong zoning characteristics, and the failure range and stress distribution range of the surrounding rock of the belt roadway in the 2103 working face of Gaojiazhuang Coal Mine are detected. Finally, the coupling strengthening support scheme combining prestressed anchor cable and bolt is proposed. The engineering application and the observation of surrounding rock deformation show that the reinforced support technology can effectively enhance the stability of the surrounding rock of the interbed roadway in Gaojiazhuang Coal Mine, and it has a good reference for the surrounding rock conditions of this kind of roadway.

1. Introduction

With the improvement of mechanization and intensification of coal mine mining, mining roadway section area is increasing, so in the construction of mining roadway, the way of breaking the bottom along the top or breaking the top along the bottom is often used to carry out the construction, resulting in the coal-rock interbed roadway proportion more and more. Interbed of coal and rock roadway surrounding rock is a thin layer of more than two of coal and rock, single layer thickness variation difference is not big, but each other between the layers of the coal-rock mechanical properties of the difference is very big, and the cementation between coal strata is weak, each layer has a certain thickness, but its relative development joint and bedding carry capacity of six to one. Due to the influence of the weak structural surface of interbed coal and rock roadway, the mine pressure becomes more intense, and the instability phenomena such as roof sinking, roadway bulging, and floor heave often occur in the roadway, which brings great difficulties to the stability control of roadway surrounding rock [1–10].

A lot of research work has been carried out by scholars at home and abroad for coal-rock interlevel roadways. Zhang used field measurement, theoretical analysis, and numerical simulation to determine the reasonable width of coal pillars in the thin coal roof face section affected by high geostress and creep damage in deep wells [11]. Feng and Zhang used the finite element dynamic software ANSYS/LS-DYNA to simulate and analyze the propagation and attenuation law of pressure waves during the blasting of coal-rock interbed masses [12]. Zhong et al. used similar simulation tests and

numerical simulation tests to study the adaptability of the inclined trapezoidal and straight-walled semicircular arched roadway to the coal and rock interbed roadway; orthogonal simulation tests were conducted to obtain 6 coal rock instability factors of interlevel roadways [13, 14]. Wei et al. studied ultrasonic imaging recognition of coal-rock interface based on the improved variational mode decomposition [15]. Shou et al. studied experimental and analytical investigation on the coupled elastoplastic damage model of coal-rock [16]. Wu and Qin studied the loose and broken distribution of soft coal rock in deep coal roadway sidewall [17]. Yang revealed the intrinsic mechanism of the weakening of the thin layered interbed roof under the action of water [18]. Cui studied the deformation characteristics of the roof roadway in the interbed roof of the soft coal seam and the interaction mechanism between the two soft sides and the deformation process of the interbed roof [19]. Qin and Shi proposed the "two soft and one hard" coal gangue interbed composite difficult-to-mined fully mechanized top coal caving mining technology for composite coal roadway support [20]. However, due to the differences in the geological occurrence and mining technology conditions of coal seams in coal mines, the instability mechanism of coal-rock interbed roadway in different areas and its support technology still need to carry out theoretical and practical research according to local conditions [21–30].

In this study, the belt roadway at the 203 working face of Gaojiazhuang Coal Mine was taken as the research object. The ultrasonic wave and numerical simulation technology were used to study the failure characteristics of the surrounding rock, detect and simulate the range of surrounding rock loose zone, analyze the instability mechanism of the roadway, optimize the existing support scheme, and propose the design technology of strengthened support, which provides a reference for the subsequent support control of roadway under similar conditions.

2. Project Overview

The designed production capacity of Gaojiazhuang Coal Mine is 3 million tons/year. There are 4 layers of coal seams in the minefield, which are No. 2, No. 4, No. 8, and No. 9 + 10 seams from top to bottom. The 203 working face is located in the first plate area of the No. 2 coal seam. The thickness of the No. 2 coal seam is 1.65 m~1.85 m with an average of 1.75 m, and the average dip angle of the coal seam is 6°. The coal seam contains 0–3 layers of gangue, which is a typical interbedded structure of coal and rock. The direct roof of the coal seam is 2.5 m thick mudstone, and the basic roof is 5.2 m thick fine sandstone. The direct bottom is 1.8 m thick mudstone, and the basic bottom is 1.1 m thick No. 3 coal seam (nonmining). See Table 1 for the lithologic characteristics of No. 2 coal seam roof and floor.

The 203 working face adopts three roadway layouts, with a strike length of 972 m and dip length of 172 m, respectively. Tape lane width and height are 4.2 m × 2.8 m, the combined support with anchor, network, in the form of roof bolt arrangement in each row for root is Φ20 × 2500 mm high strength metal bolt, the bolt between row spacing is 1200 mm × 1000 mm, the side bolt adopts Φ20 × 2200 mm right screw full thread and other strong metal bolts, the row spacing between bolts is 1100 × 1000 mm, the top steel belt is welded with Φ16 mm round steel, the side steel belt is welded with Φ12 mm round steel, the top anchor net adopts No. 10 spot welding metal net, the specification is 1000 × 2300 mm, the help net adopts No. 10 galvanized iron wire diamond net, and the specification is 1000 × 2500 mm.

Table 1: Lithological characteristics of No.2 coal seam.

Horizon	Lithology	Thickness (m)
Roof	Fine sandstone	5.2
	Direct top mudstone	2.5
Coalbed	No. 2 coalbed	1.75
Floor	Direct bottom mudstone	1.8
	No. 3 coalbed	1.1

Influenced by the occurrence condition of the coal seam, the interbedding arrangement of coal and rock along the top and bottom is adopted in the excavation of 203 working face, which brings great difficulties to roadway support. Figure 1 shows the layout of the roadway at the working face 203, and Figure 2 shows the support section of the belt roadway at the working face.

3. Research on the Failure Mechanism of Coal-Rock Interbed Roadway

The stress environment of the rock mass is a relatively balanced three-dimensional stress stable state before coal and rock interbedding roadway excavation. After the construction of the roadway, the stress in the surrounding rock is redistributed, and the stress environment is changed into a nearly two-dimensional stress state. The horizontal stress is transferred to the roof rock, and the vertical stress is transferred to the coal and rock in the two sides of the roadway. If the stress value caused by the stress concentration is greater than the rock strength, the surrounding rock will be damaged, and this failure zone is also the range of the surrounding rock loosening zone. On the contrary, the surrounding rock is in an elastoplastic state and remains stable. The intensity and stress state changes of surrounding rock before and after roadway excavation are shown in Figure 3.

As can be seen from the figure, the coal and rock mass were subjected to high primary rock stress before the roadway construction, the maximum and minimum principal stress were similar, the Mohr circle was far from the strength envelope, and the coal and rock mass in the roadway were in a stable state. After unloading, the lateral stress of the surrounding rock decreases in a certain range, and the lateral pressure drop of the surrounding rock surface is zero. At the same time, the stress is adjusted and transferred to the surrounding roadway, causing local stress concentration, increasing the maximum principal stress, and decreasing the minimum principal stress, which shows that the Moire circle is cut by the strength envelope after roadway excavation construction, and the coal and rock mass are

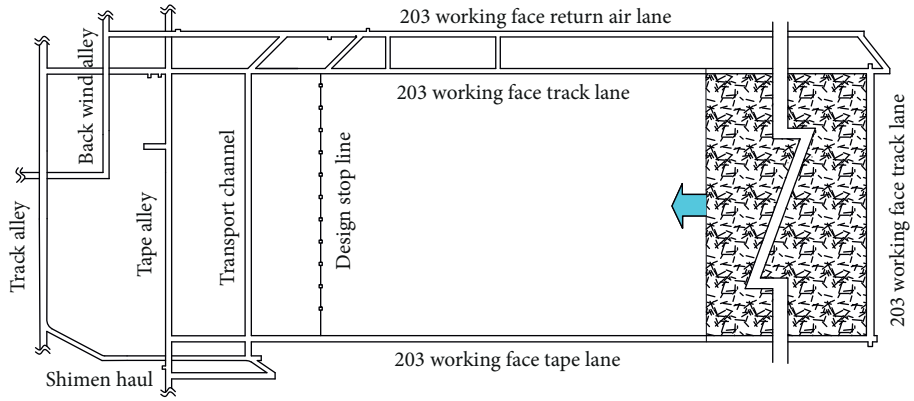

Figure 1: Roadway layout of the 203 working face.

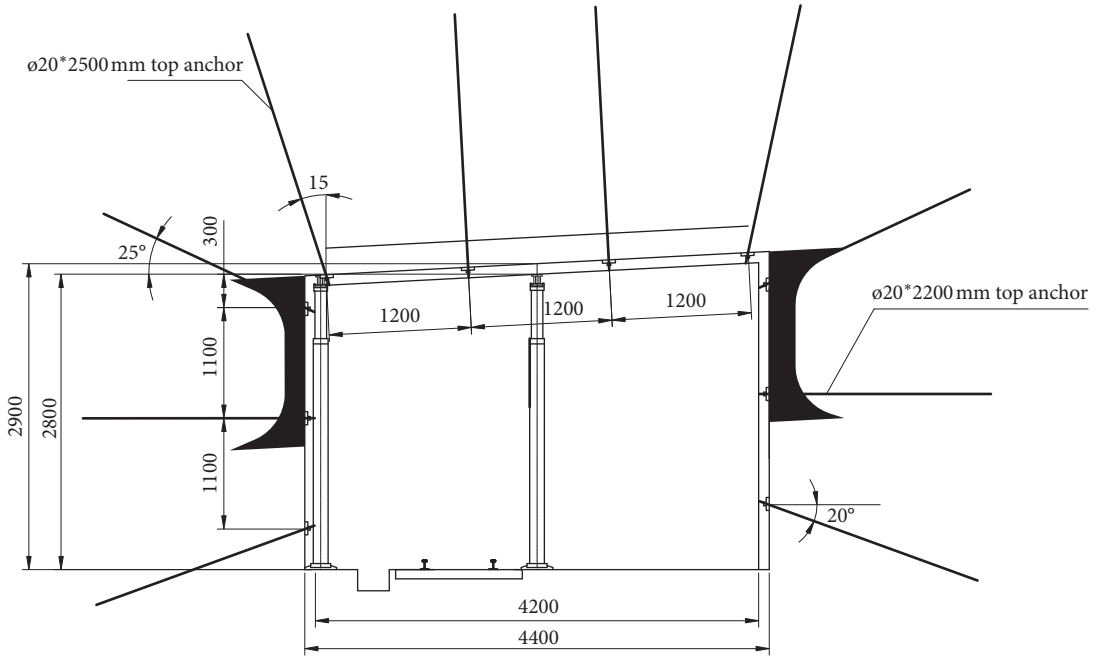

Figure 2: Sectional view of the original support of the belt lane.

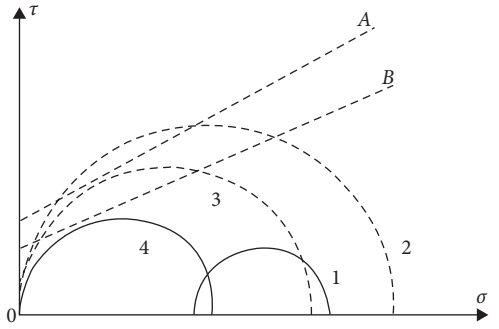

Figure 3: Changes in strength and stress of surrounding rock after the construction of the roadway. 1: raw rock stress circle; 2: deformation circle after roadway construction; 3: stress circle after roadway construction; 4: stress circle after roadway construction is stable; A: envelope line after roadway construction; B: long-term roadway stability package network.

destroyed. In order to maintain the stable state of the roadway, the first thing is to restore or improve the stress state of coal and rock mass as soon as possible after roadway construction. The timelier measures are taken; the smaller the degree of rock mass destruction, the better the integrity of coal and rock mass, and the more stable the rock mass.

According to the study, the roof of layered strata of coal measures is arched, and the failure formula of roadway surrounding rock according to the Platt pressure-free arch theory is as follows:

$$R = \left(\frac{k_c \cdot \gamma \cdot H \cdot B_c}{100\sigma_m} - 1 \right) \cdot h \cdot \tan\left(45^\circ - \frac{\phi}{2} \right). \quad (1)$$

In the formula, k_c is the stress concentration factor of the surrounding rock of the roadway, which is 2; γ is the average bulk density of the rock mass, which is 25 kN/m^3; H is the coal seam depth, corresponding to the surface elevation of +100 m, and the coal seam elevation of +510 m, then H is 590 m; B_c is the mining influence coefficient, which is 0.5; σ_m is the uniaxial compressive strength of the roof rock mass, which is 30 MPa; h is the roadway height, which is 2.9 m; φ is the internal friction angle of the coal seam, which is 64°.

The failure range of the surrounding rock of the interbedded roadway is calculated by using the data. $R = 2.61$ m.

The maximum loosening range of the roof is $b = (a + R)/f_m$, where f_m is the firmness coefficient of the roof rock layer, taking 1.9; a is the half-lane width, taking 2.1 m. Substituting the data, it is calculated that the maximum loosening range of the roof of the coal-rock interlevel roadway is 2.48 m.

The above analysis shows that the direct roof rock layer is generally mainly affected by the effect of horizontal stress. The roof rock layer with relatively low local strength is damaged due to the stress reaching the limit of failure, resulting in a wide range of shear displacements or through fractures, resulting in collapse. Therefore, in order to ensure the safety of the roadway and the stability of the surrounding rock mass, the necessary support is usually required after the construction of the roadway to limit the continuous development of the deformation and damage of the surrounding rock of the roadway, and the stress imposed by the support on the surface of the roadway surrounding rock must reach sufficient amount. However, in terms of current roadway support technology and technical level, the stress that can be applied to the surrounding rock surface of the roadway by relying solely on the support method is relatively small compared to the original rock stress of the deep rock mass. This is the fundamental reason why the traditional existing support methods are not effective in the surrounding rock of deep roadways, and it is necessary to change the inherent properties of the surrounding rock by means of reinforcement. That is, the inherent strength of the surrounding rock (cohesion and internal friction angle) is increased by means of support and reinforcement, and the bearing capacity of the surrounding rock is enhanced.

Because the inherent strength of the surrounding rock belongs to shear properties, this requires that the support plus solid itself must have a sufficiently high shear strength, and because of the brittle nature of the surrounding rock mass, it will fail as long as it undergoes small shear deformation cohesion. The supporting structure must have sufficient high shear strength and sufficient toughness to ensure that the inherent strength of the surrounding rock mass of the roadway can be significantly improved.

4. Numerical Simulation of Failure of Roadway between Coal and Rock

In this study, FLAC numerical simulation software was used for the theoretical calculation to simulate the surrounding rock failure, such as the supporting effect and stress state of coal and rock interbedding mining roadway, and theoretically reveal the deformation and failure law, stress distribution characteristics, and failure area distribution characteristics of surrounding rock of coal and rock interbedding mining roadway.

4.1. Model Establishment and Parameter Selection. The numerical simulation is based on the geological conditions of the coal seam in the 203 belt roadway. The model is 50 m in length, 54 m in height, and 30 m in width, with 118,200 units and 124,160 nodes in total, and 30 m boundaries are left around each. The numerical simulation calculation model is shown in Figure 4.

The constitutive model of numerical simulation is divided into seven layers, and the Moor-Coulomb failure criterion is selected. The physical and mechanical property parameters of each coal stratum are shown in Table 2.

4.2. Comparative Analysis of Numerical Simulation Results. As the roadway is constructed along the top and the bottom, the upper part is No. 2 coal seam with gangue layer, and the floor strata of the lower seam, the typical coal, and rock interbedding roadway conditions are formed. In order to deeply analyze the law of displacement, deformation, and stress distribution of the roadway and the supporting effect of the roadway, two cases of original support (original design) and strengthened support (follow-up design) of the roadway were, respectively, numerically simulated to provide a reference for the subsequent surrounding rock support control optimization of the roadway.

4.2.1. Analysis of Maximum Principal Stress. The cloud diagrams of the maximum principal stress distribution for numerical simulation under two different support conditions are shown in Figure 5. It can be seen from the figure that a low-stress area appears within a certain range around the excavation of the roadway, especially a large range of low-stress areas (or even a tensile stress area) in the floor of the two sides of the roadway. The tensile strength of the body is much smaller than the compressive strength, so the coal-rock mass in this area was considered to be seriously damaged. At the same time, it is worth noting that within a certain range of the roof of the roadway, a pressure arch that acts on the two sides of the roadway is formed, which also causes a local high-stress zone outside the roadway to a certain extent. In addition, it can be

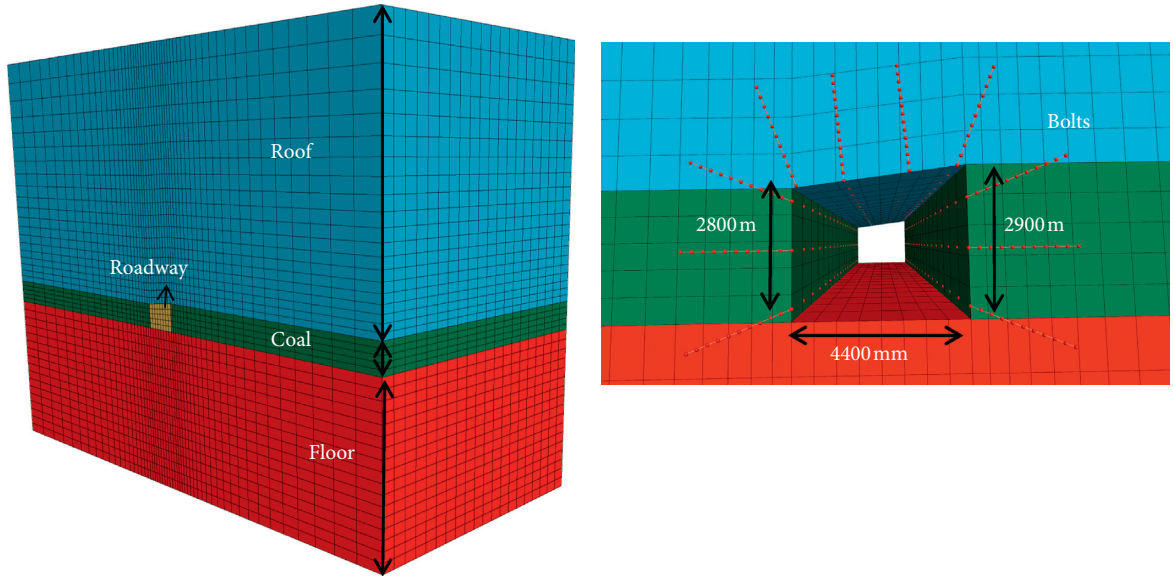

Figure 4: Numerical simulation calculation model: (a) model structure and (b) bolting parameter.

Table 2: Parameters of physical and mechanical properties of various coal and rock layers.

Model level (m)	Thickness (kg/m^{-3})	Density (MPa)	Adhesion (°)	Friction angle (GPa)	Bulk modulus (GPa)	Shear modulus (MPa)	Tensile strength
Sandstone	20	2500	16	36	16.3	13.5	2
Fine sandstone	5	2700	14	34	17.6	14.1	1.86
Direct top mudstone	4	2000	2	32	5.8	2.96	0.83
No. 2 coalbed	2	1400	0.35	18	1.15	0.33	0.15
Direct bottom mudstone	2	2000	0.86	28	3.8	1.96	0.45
No. 3 coalbed	1	1400	0.35	18	1.15	0.33	0.15
Sandstone	20	2500	16	36	16.3	13.5	2.2

seen that the roadway support measures have reduced the low-stress area of the roadway roof to a certain extent and have a small impact on the low-stress area of the roadway gang, and to a certain extent, the low-stress area of the roadway floor has been increased.

4.2.2. Analysis of Deformation of Surrounding Rock of Roadway. The vector diagram of the surrounding rock deformation of the roadway under two different support conditions is shown in Figure 6. The length of the arrow line in the figure indicates the magnitude of the displacement vector at that point, and the direction of the arrow indicates the vector direction of the point displacement. It can be seen from the figure that after the roadway is excavated, the two sides of the roadway have the largest continuous deformation of the coal and rock mass, followed by the roadway floor, and the continuous deformation of the roadway roof is relatively small. The reason for this analysis is that due to the hard lithology of the roof of the roadway, a pressure-bearing arch structure is formed above the roadway (the existence of the pressure arch can be seen from the above maximum principal stress cloud diagram), so the absolute deformation of the roof is not large.

4.2.3. Analysis on the Law of Roof Subsidence of Roadway. See Figure 7 for the cloud subsidence of the roof of the roadway under two different support conditions, and see Figure 8 for the graph of roof subsidence and reduction rate. It can be seen that the subsidence curve of the roof of the roadway after the excavation of the roadway has an inflection point at the roof of 4 m, and the subsidence of the roof of the roadway within 4 m is significantly greater than that of the roof above 4 m. Strengthened support compared with the original support scheme, the original support is not as effective as strengthening support in reducing the roof subsidence rate within 2.5 m, and the original support is more powerful than the supporting roof when the rock layer is 2.5 m away. The sink reduction rate is large.

4.2.4. Analysis of the Distribution Law of the Surrounding Rock Elastoplastic Zone. The distribution of the elastoplastic zone of the surrounding rock of the roadway under two

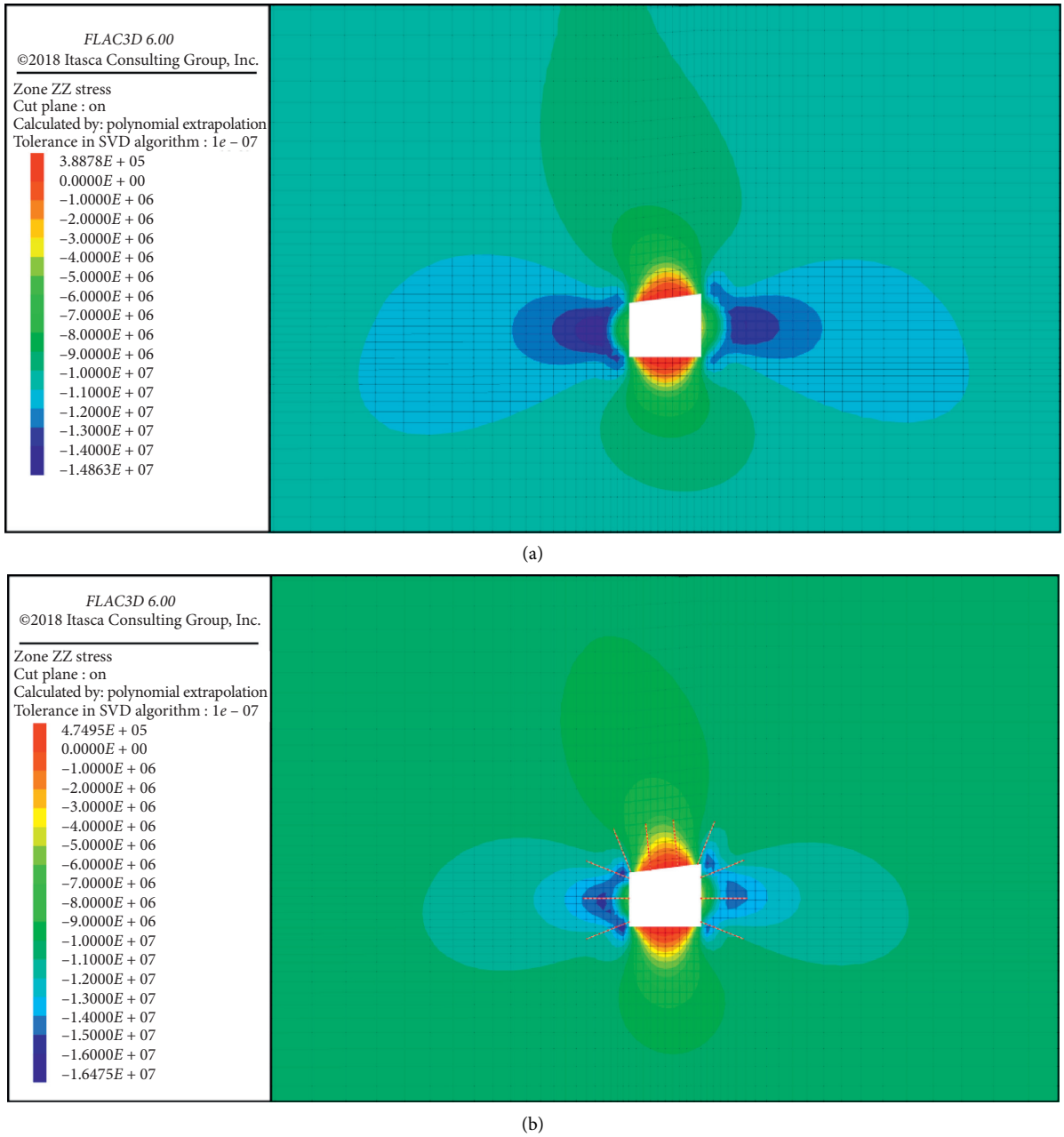

Figure 5: Cloud diagram of maximum principal stress distribution in numerical simulation: (a) original support and (b) reinforced support.

different support conditions is shown in Figure 9, where different colors indicate different plastic states (such as tensile plastic zone and shear plastic zone). It can be seen from the figure that after the excavation of the roadway, a large plastic area appears in the two corners of the roadway and a certain range of the roof, and the plastic area of the roof is arched. This is the same as the support pressure above the roof of the roadway obtained from the above-mentioned main stress distribution cloud diagram. Arch simulation wants to fit. This is also consistent with the lithological characteristics of the roof of the roadway mentioned above, but the brittleness of the roof due to the characteristics of the roof results in the local deformation of the roof under the condition of a small amount of deformation, so that the entire large area of the pressure arch occurs.

4.3. Analysis of Surrounding Rock Failure Characteristics Revealed by Numerical Simulation. Compared with the rock strata, the coal seam is the weaker structure of the surrounding rock of the roadway, and its deformation is greater than that of the rock strata, which is also the reason for the large deformation of the coal body at the roadway side. Figure 10 shows the comparison of deformation distribution of different media in surrounding rock of interbedded roadway. For the interbedding coal and rock mining

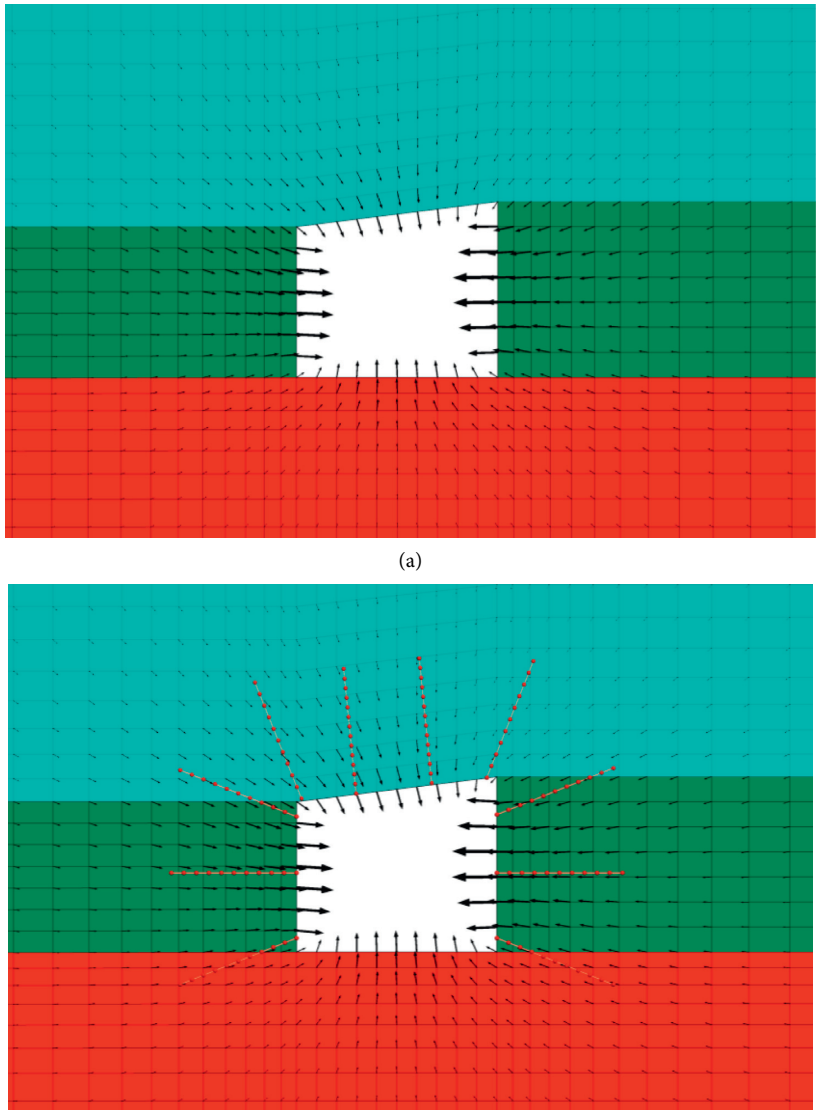

(a)

(b)

Figure 6: Vector diagram of deformation of surrounding rock: (a) original support and (b) reinforced support.

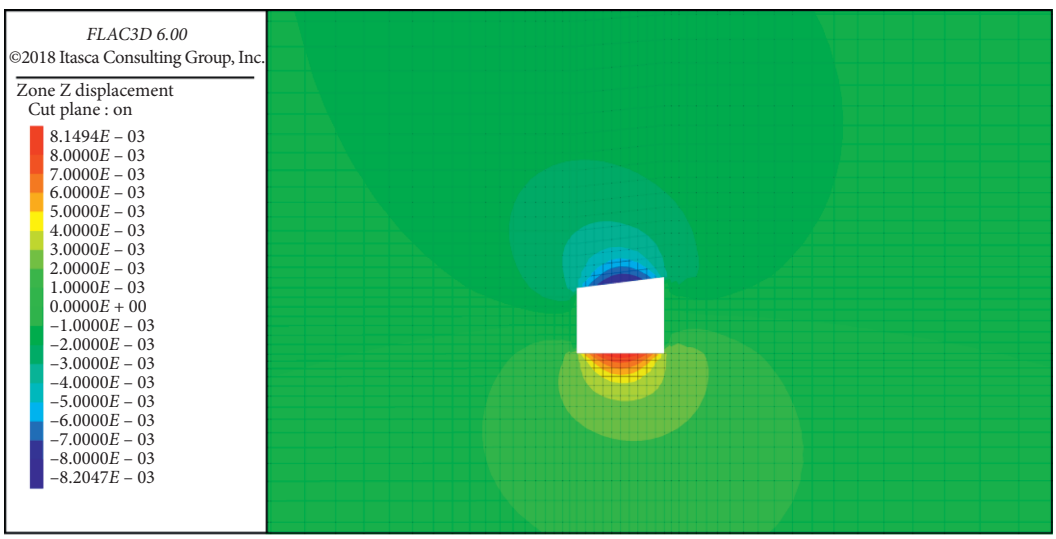

(a)

Figure 7: Continued.

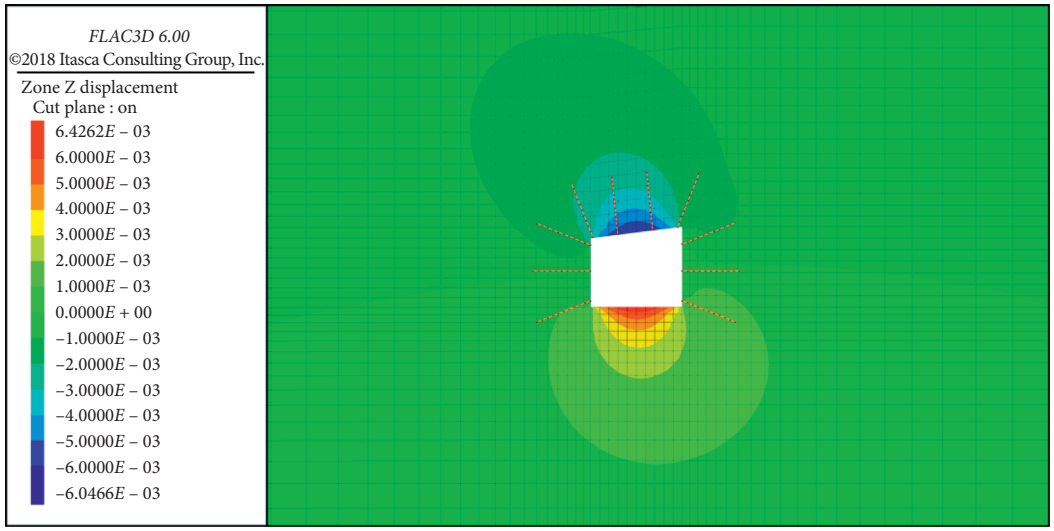

(b)

Figure 7: Sinking clouds on the roof under different support conditions: (a) original support and (b) reinforced support.

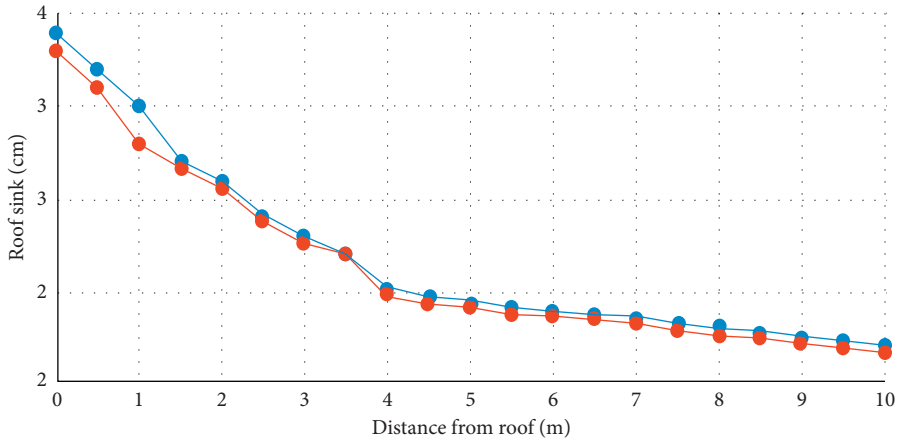

(a)

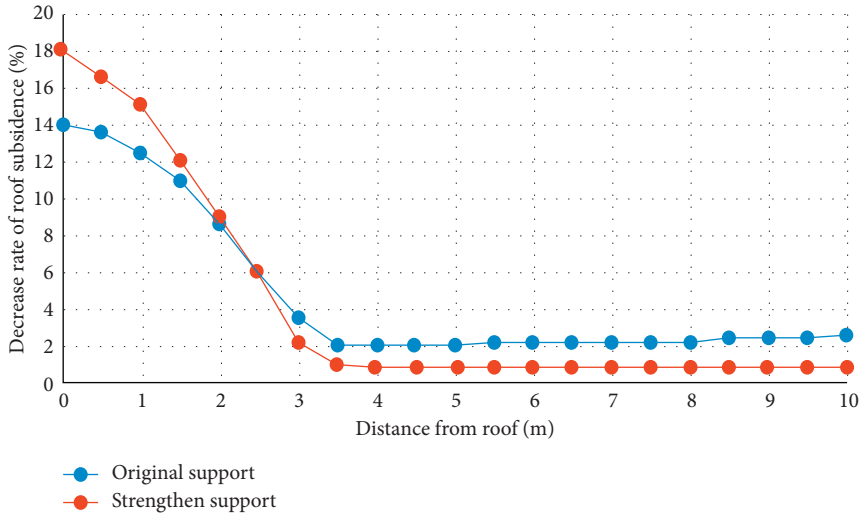

(b)

Figure 8: Curve of roof subsidence and reduction rate under different support conditions. (a) Graph of roof subsidence and (b) Graph of a reduction rate of roof subsidence.

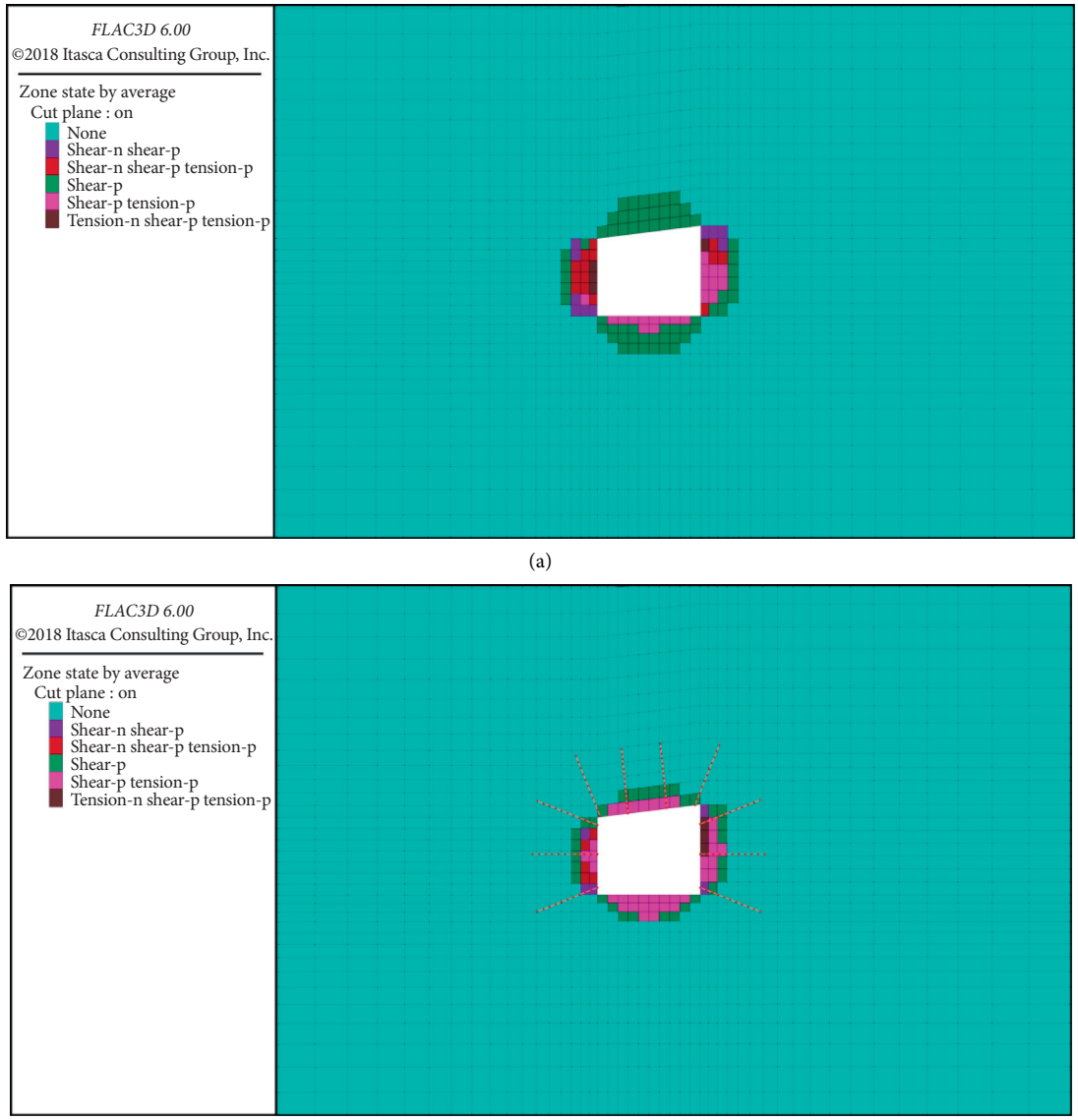

Figure 9: Distribution law of surrounding rock elastoplastic zone of the roadway with different support conditions: (a) original support and (b) reinforced support.

roadway at the 203 working face, different support schemes can control the deformation of surrounding rock to a certain extent. Compared with the original support scheme, the enhanced support has a more obvious control effect on the deformation of surrounding rock in the roadway to a certain extent, while the control effect of the shallow near field surrounding rock is not obvious.

5. Ultrasonic Detection of Coal-Rock Interbed Roadway Failure

5.1. Technical Principles. According to the rock mechanics theory, the integrity of the surrounding rock is good, its compressional wave velocity is high, the surrounding rock joints and fractures are more or more broken, and its compressional wave velocity is low. Therefore, the characteristic parameters such as wave velocity, amplitude, and frequency of the ultrasonic longitudinal wave and their change rules are measured in the underground, so as to judge the lithology, density, cracks, weak interlayer, and other states and analyze the range of the loose zone of roadway surrounding rock.

A probe of a double-receiver transducer is placed in the borehole, and the transmitting transducer F emits ultrasonic waves in the borehole, generating gliding waves around the borehole wall to propagate along the borehole. Receiving transducers 1 (S1) and 2 (S2) receive the first wave of gliding wave, respectively. Therefore, the propagation velocity can be obtained according to the propagation time from the transmission to the receipt of the first wave recorded by the single-chip microcomputer and the fixed propagation distance between probes according to propagation

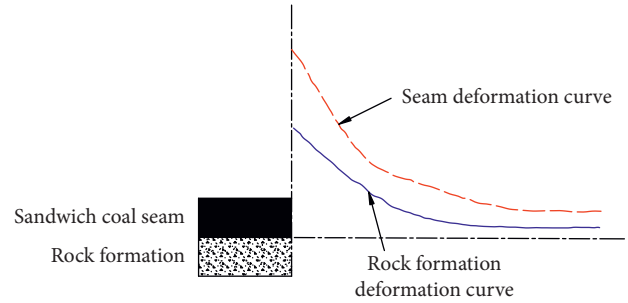

Figure 10: Comparison of deformation distribution of surrounding media in surrounding rock of coal-rock interbed roadway.

velocity = propagation distance/propagation time, and then the boundary of the loose circle can be determined by using it. The principle diagram of the ultrasonic crack tester for the surrounding rock is shown in Figure 11.

5.2. Ultrasonic Scene Detection Scheme

5.2.1. Instrument and Detection Method. The drill was drilled with a CLC1000 tester, with a diameter of 45 mm and a distance of 0.1 m between the transmitter and receiver. The drilling hole was tested in time after forming. The drilling hole was rinsed with pressure water before testing and the coal powder was cleaned. After the tester is connected with the probe, the probe is sent to the bottom of the hole with a push rod, and then the pushrod is pulled to record the sound wave outward at 10 cm for each block until the mouth of the hole. See Figure 12 for the layout of detection stations for surrounding rock failure of the roadway.

5.2.2. Arrangement of Measuring Points in Underground Roadways. Considering the current mining position of the working face and other influencing factors, the belt roadway of the 203 working face is selected as the object of underground exploration. The position of the detection points for surrounding rock failure is arranged at a distance of 70 m from the current position of the working face of the belt roadway. See Figure 13 for the layout plan of the detection points. A group of boreholes are arranged every 30 m for testing, consisting of 3 groups of measuring points, and 4 boreholes are arranged at each group of measuring points, which are, respectively, located in the middle of the waistline on both sides of the roadway and the floor. The two sides of the holes are arranged in the waistline position of the two sides of the roadway. The hole depth is 6-7 m, the diameter is 45 mm, and the bottom of the hole is inclined downward about 8–10°. The empty floor is arranged in the middle of the roadway floor, perpendicular to the roadway floor, with a hole depth of 6-7 m and a diameter of 45 mm. See Figure 14 for the horizontal section of the detection borehole at the detection point.

5.3. Research on Ultrasonic Field Detection Results. The purpose of underground ultrasonic detection is to find out the failure range and stress distribution range of surrounding rock of interbedded roadway. See Figure 15 for ultrasonic detection results of cracks in surrounding rock of roadway at different leading positions from 203 working face.

The following can be seen from Figure 15:

(1) The wave velocity at the side of the coal pillar at a distance of 70 m from the working face drops sharply in the range of 0.9 m–1.2 m in borehole depth, and the wave velocity decreases from 1085 m/s to 900 m/s. The wave velocity at the side of the coal pillar 100 m from the working face dropped sharply at the depth of 1.8–2.0 m, and the wave velocity dropped from 1148 m/s to 970 m/s. There is no significant change in the side wave velocity of the coal pillar at a distance of 130 m from the working face

(2) The wave velocity of the solid coal side 70 m away from the working face drops sharply at a drilling depth of 0.9, and the wave velocity decreases from 1160 m/s to 1080 m/s; in addition, the range of 5.0–5.9 m also fluctuates violent fluctuations. The wave velocity of the solid coal side 100 m away from the working face drops sharply at a depth of 1.1 m, and the wave velocity drops from 1132 m/s to 1115 m/s. The wave velocity drops sharply at a depth of 3.1 m–3.6 m, and the wave velocity is s dropped to 1088 m/s; a sharp drop occurred in the borehole depth range of 4.2 m–4.5 m, and the wave velocity dropped from 1120 m/s to 1078 m/s. There is no significant change in the side wave velocity of the solid coal at a distance of 130 m from the working face

(3) From the above analysis, it can be seen that the wave velocity of the coal pillar side is significantly lower than that of the solid coal side. The stress concentration range of the coal pillar side of the belt lane in the 203 working face is between 0.9 m and 2.0 m, the stress concentration range caused by the solid coal side is 0.9–1.1 m, and the range of 3.1–4.5 m on the side of the solid coal is also obvious

The schematic diagram of the surrounding rock failure stress distribution range of the coal-rock interbed roadway revealed by the detection of the belt lane in 203 working face is shown in Figure 16. The results of stress observation show that under the condition of the existing support system, about 0–2 m of the surrounding rock failure of the 203 belt lane is the loosening circle of the surrounding rock, and

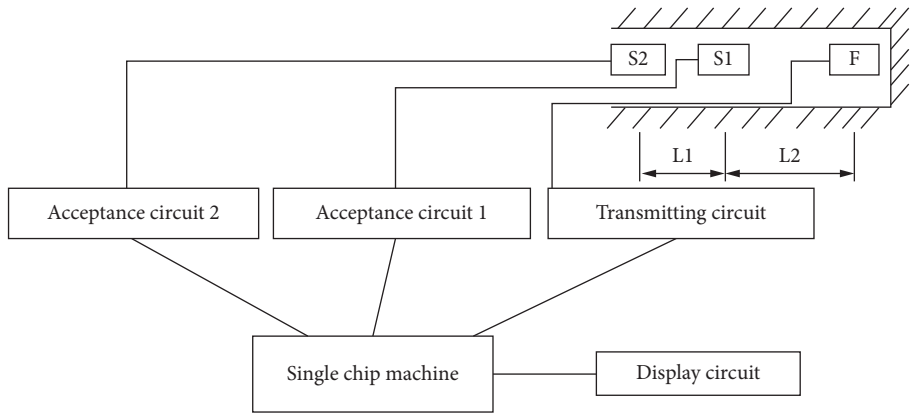

Figure 11: Schematic diagram of ultrasonic surrounding rock fracture tester.

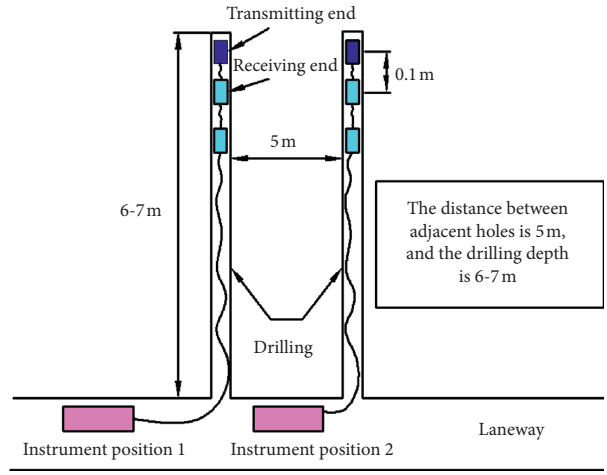

Figure 12: Arrangement of roadway surrounding rock damage detection stations.

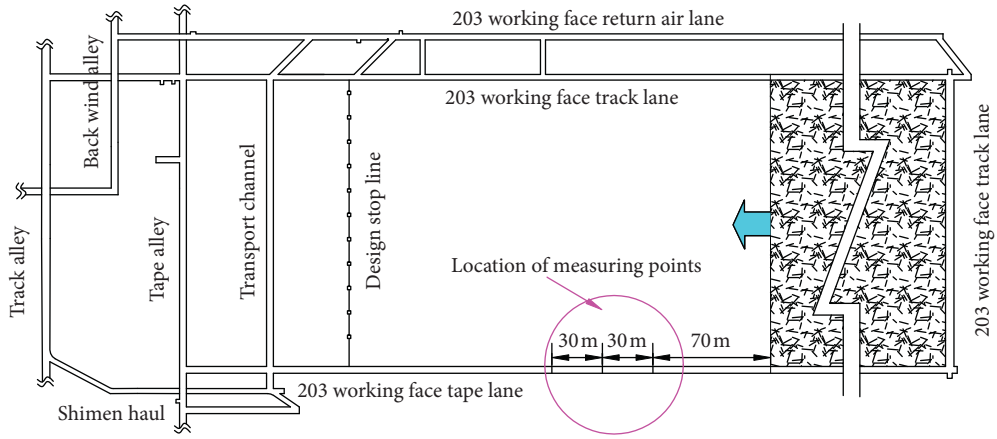

Figure 13: Plan view of measuring point arrangement position.

about 2.0–3.1 m of the surrounding rock failure of the laneway is the effect of the anchor to support the impact. In the region, the range of about 3.1–4.5 m destroyed by the surrounding rock of the roadway is the plastic zone, which is the influence range of the external stress field revealed by the foregoing numerical simulation results.

5.4. Analysis of Surrounding Rock Failure Characteristics Revealed by Ultrasonic Detection. Through the ultrasonic detection of the surrounding rock, the failure characteristics of surrounding rock revealed by the ultrasonic detection results of surrounding rock fractures are shown in Figure 17. The results show that the coal seam is affected by the internal

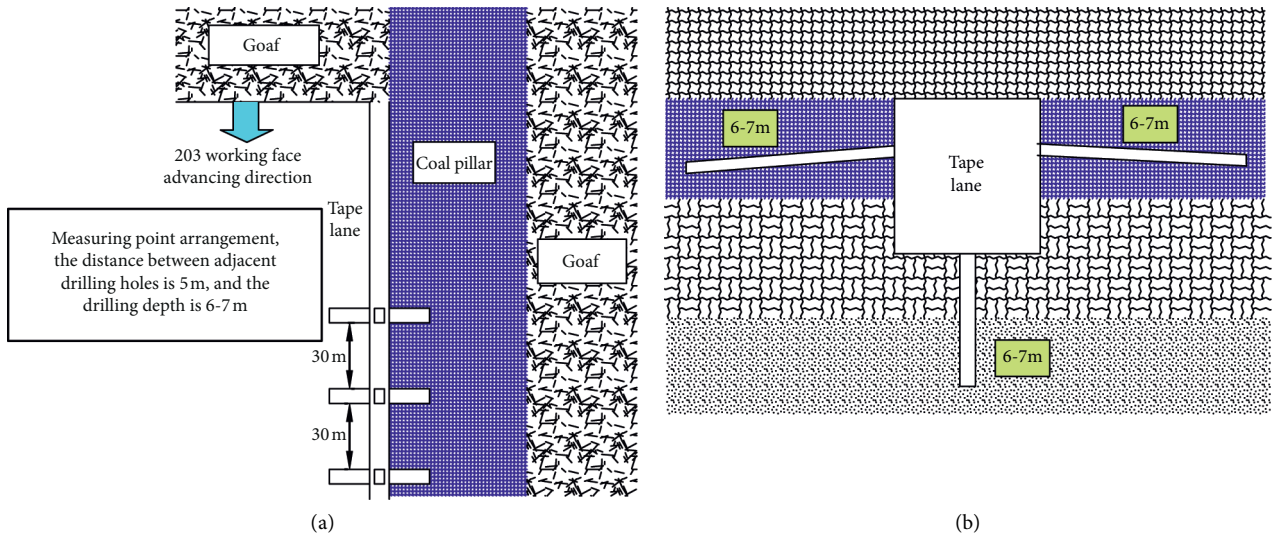

Figure 14: Plane section of borehole survey: (a) floor plan and (b) section.

and external stress field, and the failure range is large, with strong zoning characteristics. From near to far, the coal wall of the roadway is, respectively, the range of surrounding rock loose zone, the range of near field fracture under the control of bolt support, the range of far-field fracture without the influence of bolt support, and the stress area of the original rock. In the range of the above several fracture distribution areas, roadway bolt support can only control the range of near field fractures, and the development of the loose circle range is greatly affected by the support prestress, which is also the key range of bolt support control at present. In order to control the large deformation of surrounding rock, it is necessary to control the development of near field cracks, increase the strength of support, or strengthen the bearing capacity of the coal seam.

6. Design of Enhanced Support for Coal-Rock Interlevel Roadway

6.1. Strengthening the Theoretical Basis of Support. Through the above theoretical analysis, numerical simulation, ultrasonic detection, and other methods, it is obtained that the failure height of the 203 belt lane is 2.48 m, 2.5 m, and 2.0 m, respectively. The maximum value of 2.5 m is taken as the reference value of the surrounding rock failure support of the 203 belt roadway. Due to the small strength of the roof and easy destruction of the 203 belt roadway, the damage range of mudstone roof strata in the roadway is large, and the roof strata are the key point of the strengthened support design. The original rooftop anchor rod specifications for Φ 20×2500 mm obviously cannot satisfy the need for safety and must strengthen the supporting design. See Figure 18 for the schematic diagram of roof rock instability under the control of original bolt support.

According to the site conditions, due to the use of the original design of the original anchor support in the 203 belt lane, the phenomenon of severe local roof sinking was brought about, and the mine pressure was more obvious. According to the characteristics of this type of roof of coal and rock interbed, a prestressed anchor cable and anchor rod combined strengthening support scheme is adopted; that is, on the basis of ordinary anchor rod support, the roof is reinforced by installing anchor cables along appropriate sections. The mechanism is as follows: (1) the anchor cable strengthens the roof rock layer farther above into a peripheral load-bearing arch with a strong bearing capacity, that is, the "outer bearing arch"; (2) the "outer bearing arch" can not only maintain its own stability; it also becomes the foundation for the stability of the balanced arch supported by the lower anchor support; (3) through a certain spacing, the anchor cable will make the outer arches along the shape overlap each other and maintain the rock mass within the range of "outer bearing arch". *Overall Stability*. A schematic diagram of the strengthening mechanism of the roof rock layer under the combined support of the anchor cable and anchor rod is shown in Figure 19.

6.2. Anchor Cable Reinforced Support Design

6.2.1. Anchor Cable Length Design. The design length of the anchor cable should satisfy

$$L = La + Lb + Lc + L\ d, \tag{2}$$

where L is the total length of the anchor cable, m; La is the anchoring length of the anchor cable to the more stable rock formation, $L_a \geqq Kd1f_a/4f_c$, where K is the safety factor; taking 2, d_1 which is the anchor diameter is 17.8 mm; f_a which is the anchor tensile strength is 1920 N/mm^2; f_c is the adhesion strength of anchor cable and anchoring agent, N/mm^2; taking 1. Substitute the data $La = 2.56$ m, L_b is the thickness of the unstable rock layer to be suspended, 2.5 m; L_c is the thickness of the supporting plate and anchorage, taking 0.014 m; L_d is the exposed tensile length, generally 0.3 m; then, the total length of the anchor cable $L = 5.1$ m.

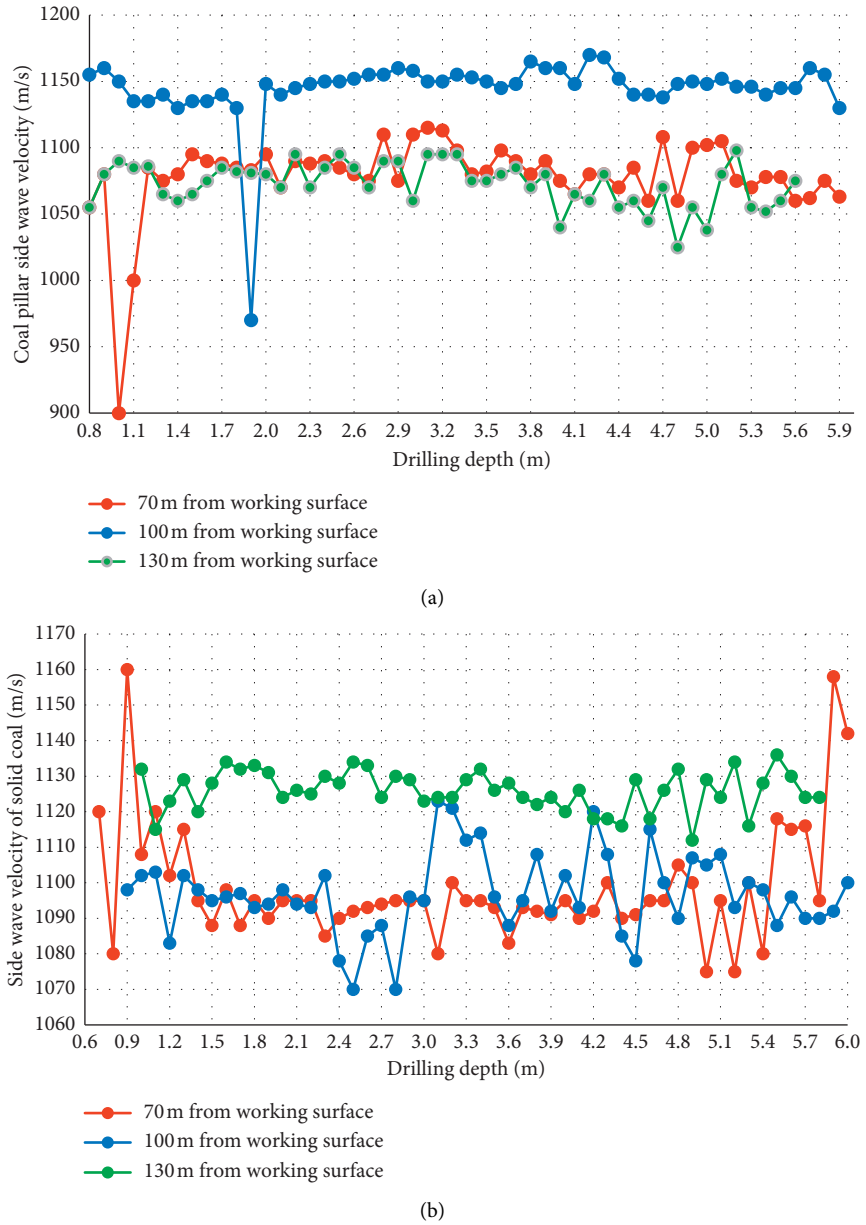

Figure 15: Ultrasonic detection results of the surrounding rock cracks in the roadway at different advanced positions from the 203 working face: (a) coal pillar side and (b) solid coal side.

According to the common specifications of anchor cables, the 6.0 m anchor cable is selected to meet the length requirements.

6.2.2. Number of Anchor Cables. The number of anchor cables should satisfy

$$N \geq \frac{KW}{P}, \tag{3}$$

where N is the number of anchor cables and K is a safety factor of 1.2.

Break P is the minimum breaking force of the anchor cable, taking 355 kN.

W is the dead weight of the suspended rock; $W = B \times \Sigma h \times \Sigma \gamma \times D$, where B is the lane width 4200 mm; D is the anchor spacing, 2000 mm; Σh is the hanging rock thickness, 5.7 m; $\Sigma \gamma$ is the hanging rock The average bulk density is 12 kN/m^3. Substitute the data $W = 575$ kN.

Then, the number of anchor cables is $N = 1.94$, and two rows of anchor cables are arranged reasonably. Figure 20 shows the sectional drawing of the reinforced anchor cable support design.

7. Strengthening Support Effect Test

On the basis of the foregoing theoretical research results, combined with the roof and roof features of the 203 belt lane

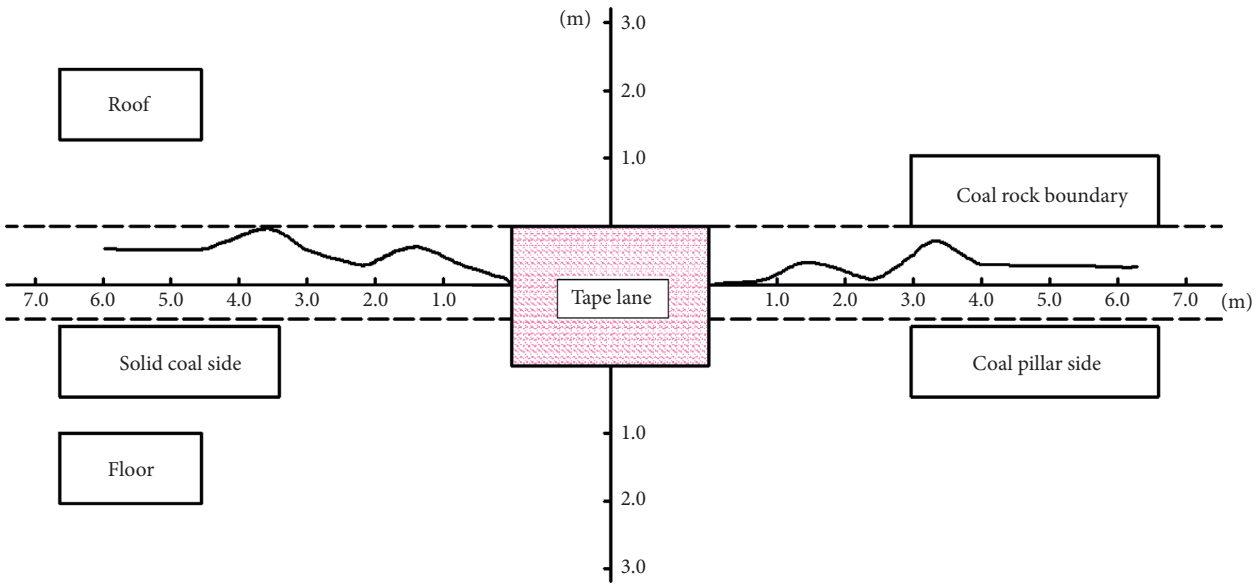

Figure 16: Schematic diagram of the surrounding rock failure stress distribution range of coal-rock interbed roadway.

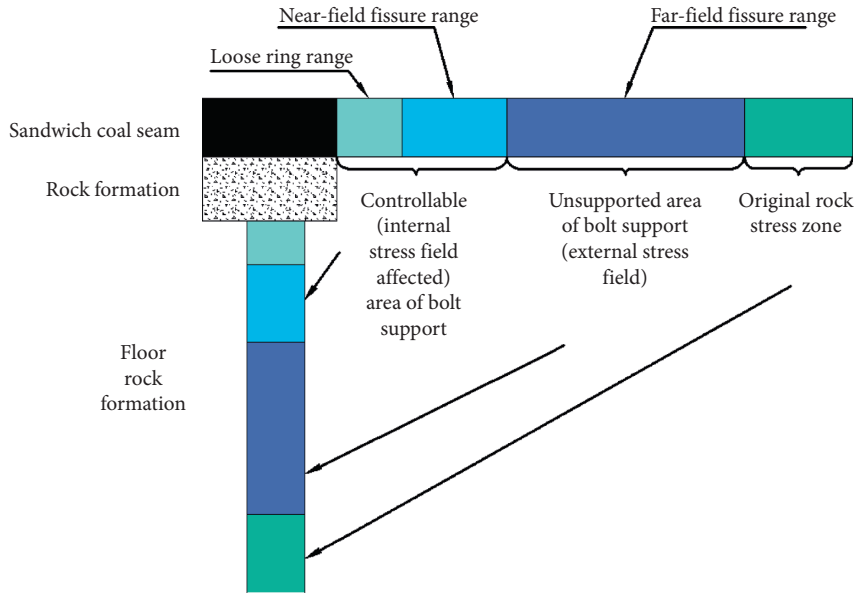

Figure 17: Schematic diagram of surrounding rock failure characteristics revealed by ultrasonic detection results.

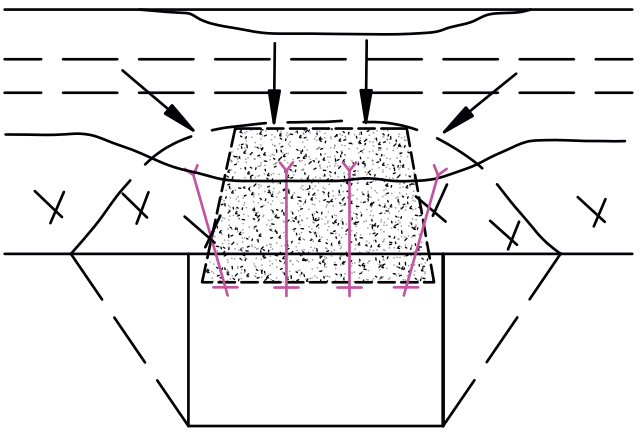

Figure 18: Schematic diagram of the instability of roof rock layer under original anchor support.

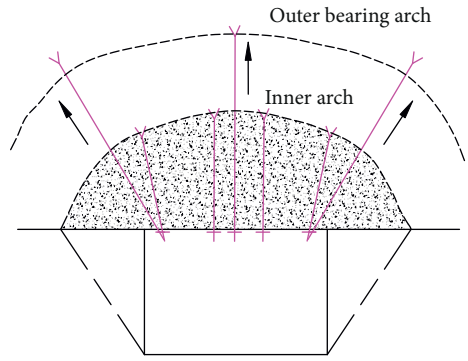

Figure 19: Schematic diagram of the strengthening mechanism of the roof rock layer under the combined support of the anchor cable and anchor rod.

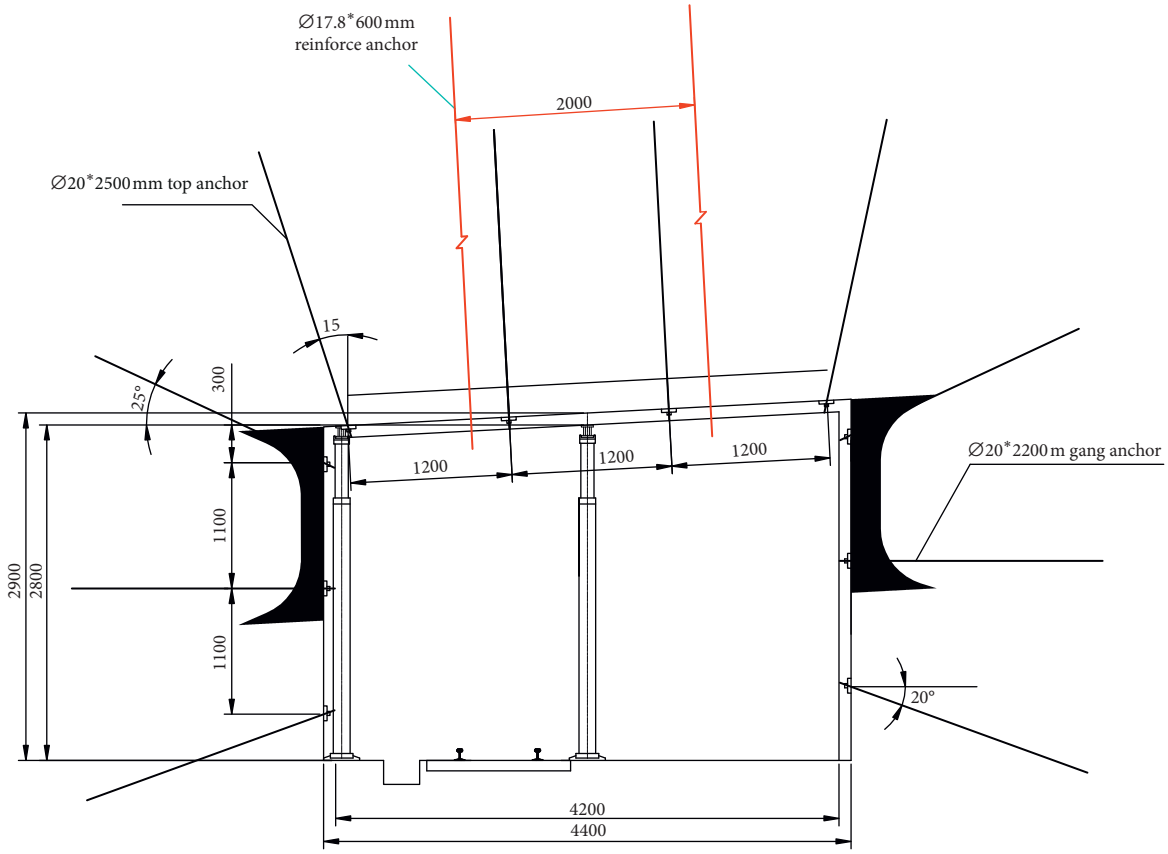

Figure 20: Sectional view of anchor cable reinforced support design.

in the field, the reinforced support design was carried out during the construction of the roadway, and the deformation of the roadway was observed. With the construction of the working face, an observation point is arranged at an interval of 50 m, and the deformation of the surrounding rock of the roadway is observed using the cross-point method. The observation period is 6 months, once a day for the first two months, and once a week for the next four months.

Observation results show that the approach distance of the roof and floor of the belt lane is 5.34 mm, which greatly improves the effective support strength of the coal-rock interbed roadway (compared with the approach distance of the roof and floor of the roadway which is 56.2 mm), which has reached the expected goal, indicating that by strengthening the support the scheme significantly improves the effect of controlling the deformation of surrounding rocks to a certain extent.

8. Conclusion

Through the research of this paper, the main conclusions are as follows:

(1) The excavation of the roadway disrupts the balance of the surrounding rock and forms the stress

concentration of the surrounding rock of the roadway. For the surrounding rock of the roadway with the characteristics of coal-rock interbed, the horizontal stress in the roof rock layer increases with the depth of the two groups of surrounding rocks. Transferring to the deep, there is a destruction of the top rock formation. Based on the analysis of Platts pressure-free arch theory, the maximum loosening range of the roof of the coal-rock interlevel roadway was obtained, which provided strong support for the rational design of the support process

(2) The failure characteristics of the surrounding rock in the coal and rock interbedding roadway were analyzed by using the numerical simulation technology, and the deformation and failure law, stress distribution characteristics, and failure area distribution characteristics of the surrounding rock in the coal and rock interbedding roadway were theoretically revealed. Although the theory and hypothesis based on the numerical simulation are limited, and the simulation results are approximate numerical solutions, the research results can provide important references for in-depth analysis of the displacement, deformation, and stress distribution law of the roadway and the supporting effect of the roadway

(3) The ultrasonic detection of the surrounding rock of the roadway shows that the coal seam is affected by the internal and external stress fields and has strong zoning characteristics. The damage range and stress distribution range of the surrounding rock of the coal-rock interbed roadway are reasonably analyzed to evaluate the surrounding rock of the roadway

(4) Based on the methods of theoretical analysis, numerical simulation, and ultrasonic detection, the comprehensive development height of the roof of the coal-rock interlevel roadway is comprehensively obtained. Based on this, a reasonable anchor cable reinforcement support design is carried out, and the analysis of the anchor cable reinforcement support is analyzed. *Mechanism of Action.* After 6 months of mine pressure observation practice, the surrounding rock of the roadway has reached the expected stability target, and the enhanced support scheme has significantly controlled the deformation of the surrounding rock to a certain extent

Data Availability

The data used to support the findings of this study are available from the submitting author upon request.

Conflicts of Interest

The authors declare no conflicts of interest.

Acknowledgments

The work was supported by the National Natural Science Foundation of China (Grant no. 51774122).

References

[1] J. Liu, N. Wu, G. Si, and M. Zhao, "Experimental study on mechanical properties and failure behaviour of the pre-cracked coal-rock combination," *Bulletin of Engineering Geology and the Environment*, vol. 11, pp. 1–15, 2020.

[2] Y. Zhang, J. Panshi, and Y. Wu, "Study on deformation and failure mechanism and support technology of mining roadway in repeated mining of steeply inclined coal seam," *Coal Engineering*, vol. 2, pp. 91–95, 2020.

[3] X. Liu, G. Yan, and Y. Zhang, "Research on failure mechanism of tunnel composite structure and control technology of bolt-grouting support," *Mining Safety and Environmental Protection*, vol. 6, pp. 102–106, 2020.

[4] Y. Chu, G. Ren, C. Zou et al., "Research on instability analysis and control method of roadway in ore contact zone," *Journal of Wuhan University (Engineering Science Edition)*, vol. 11, pp. 975–980, 2019.

[5] P. Wang, T. Feng, Y. Jiang et al., "Instability mechanism of surrounding rock in weakly reclaimed roof roadway and its control principle and technology," *Chinese Journal of Coal*, vol. 10, pp. 2953–2965, 2019.

[6] J. Sun, "Failure mechanism and support technology of roadway with weak coal and rock composite roof," *Coal Mine Safety*, vol. 9, pp. 96–100, 2019.

[7] Y. Peng, S. Zhang, and Y. Zhang, "Deformation and failure mechanism of surrounding rock in coal mine large cross section top coal roadway," *Coal Mine Safety*, vol. 5, pp. 263–268, 2019.

[8] X. Liu, *Study on Failure Mechanism and Control Technology of Composite Roof in Medium-Thick and Weak Rock Layer Type*, Taiyuan University of Technology, Taiyuan, China, 2019.

[9] B. Zhou, *Study on Instability Mechanism and Safety Control of Weak Structure on Roof of Roadway*, Anhui University of Science and Technology, Huainan, China, 2017.

[10] L. He, *Stability Mechanism and Control of Roof Roadway in Weak Coal and Rock Interbed*, China University of Mining and Technology, Xuzhou, China, 2013.

[11] Y. Zhang, "Numerical study on reasonable width of creep coal pillars in deep well and high geostressed coal-rock interbed thin roof section," *Mining Safety and Environmental Protection*, vol. 1, pp. 28–32, 2019.

[12] F. Hui and H. Zhang, "Numerical simulation of icoal-rock interbed blasting based on ANSYS/LS-DYNA," *Mining Technology*, vol. 5, pp. 128–130, 2017.

[13] Z. Zhong, Y. Li, T. Wang et al., "Simulation test and control countermeasures of coal-rock interbed roadway," *Journal of Liaoning Technical University (Natural Science Edition)*, vol. 5, pp. 555–560, 2015.

[14] Z. Zhong, X. Li, Q. Yao et al., "Study on instability factors of roof roadway in coal and rock interbed based on orthogonal test," *Journal of China University of Mining & Technology*, vol. 2, pp. 220–226, 2015.

[15] W. Wei, L. Li, W. f. Shi, and J. p. Liu, "Ultrasonic imaging recognition of coal-rock interface based on the improved variational mode decomposition," *MeasurementVolume*, vol. 170, Article ID 108728, 2020.

[16] Y. Shou, J. Zhang, and F. Berto, "Experimental and analytical investigation on the coupled elastoplastic damage model of coal-rock," *Fracture and Structural Intregrity*, vol. 14, no. 53, pp. 434–445, 2020.

[17] D.-y. Wu and S. Qin, "Loose and broken distribution of soft coal-rock in deep coal roadway Sidewall," *Geotechnical and Geological Engineering*, vol. 5, pp. 1–10, 2020.

[18] J. Yang, *Surrounding Rock Control Mechanism and Technology of Roof Tunnel in Thin-Bedded Coal-Rock Interbed*, China University of Mining and Technology, Xuzhou, China, 2013.
[19] L. Cui, *Study on Underground Pressure Characteristics and Anchoring Scheme of Roof Roadway in Soft Coal Interbed*, Taiyuan University of Technology, Taiyuan, China, 2016.
[20] X. Qin and Q. Shi, "Analysis of "two soft and one hard" coal gangue interbed composite coal roadway support technology," *Gansu Science and Technology*, vol. 13, pp. 56–59, 2014.
[21] M. Guo, P. Gong, and P. Li, "Study on the parameters of reinforcement and support of the lower roadway in the goaf of an extremely close distance coal seam," *Coal Engineering*, vol. 1, pp. 54–58, 2020.
[22] Z. Fu, X. Zeng, D. Ouyang et al., "Research on surrounding rock deformation and reinforcement support of coal mine roadway," *Coal Technology*, vol. 1, pp. 53–56, 2020.
[23] T. Jing, "Research on strengthening support of roadway under complex geological conditions," *Energy and Energy Conservation*, vol. 12, pp. 84-85, 2019.
[24] Y. Han and Z. Cai, "Research on surrounding rock reinforcement support technology in high ground pressure and three soft mining roadways," *Journal of Science & Technology and Economy*, vol. 29, pp. 47–49, 2018.
[25] X. Wang, Y. Wang, and D. Zhang, "Research on strengthening support technology for key parts of roadway with large dip angle "three soft" coal seam," *Journal of Mining and Safety Engineering*, vol. 2, pp. 208–213, 2017.
[26] B. Liu, "Technology and research on strengthening support of large-section soft rock composite roof," *Coal and Chemical Industry*, vol. 7, pp. 52–55, 2016.
[27] G. Chen, T. Li, G. Zhang et al., "Experimental study on energy accumulation before coal rock mass failure," *Journal of China Coal Society*, vol. 11, 2020.
[28] G. Chen, T. Li, L. Yang et al., "Mechanical properties and failure mechanism of different coal-rock ratios and combinations," *Journal of Mining And Strata Control Engineering*, vol. 1, 2021.
[29] G. Zhang, C. Zang, M. Chen et al., "Ground response of entries driven adjacent to a retreating longwall panel," *International Journal of Rock Mechanics and Mining Sciences*, vol. 138, 2021.
[30] G. C. Zhang, Z. J. Wen, S. J. Liang et al., "Ground response of a gob-side entry in a longwall panel extracting 17 m-thick coal seam: a case study," *Rock Mechanics and Rock Engineering*, vol. 53, no. 2, pp. 497–516, 2020.